

# Application of a Helium-Cooled Cryo-Electron Microscope for Single Particle Analysis

Kaoru Mitsuoka

Biomedical Information Research Center,  
National Institute of Advanced Industrial Science and Technology

Single particle analysis can determine three-dimensional structures of biological molecules at high resolution without the crystals. The principle obstacle for high-resolution structural analysis in electron microscopy is irradiation damage of the biological specimen, and cooling the specimen to cryogenic temperatures can reduce the effects of irradiation damage. To achieve higher resolution structures by reducing the irradiation damage, even in single particle analysis, a new cryo-electron microscope with a liquid helium-cooled stage for single particle analysis was developed, and we utilized it in two studies using single particle analysis. For the application, we slightly modified the sample preparation technique developed for the high-resolution image collection from the tubular crystals, using the liquid helium-cooled stage. The first application was to determine the structure of the GroEL-GroES-substrate complex from *Thermus thermophilus*. We observed a density corresponding to the folding substrates inside the complex. The second application was the three-dimensional reconstruction from tubular crystals of a membrane protein, human erythrocyte band 3. Iterative helical real-space reconstruction, which is a modification of single particle analysis for tubes with helical symmetry, was used for this purpose. These two examples clearly show that the three-dimensional structures of a broad range of targets can be analyzed by single particle analysis.

## Introduction

Cryo-electron microscopy (cryo-EM) is a powerful tool in structural biology for a broad range of targets and resolutions. Electron crystallography can yield maps with better than 2 Å resolution from two-dimensional (2D) crystals of membrane proteins [1]. Tubular crystals of membrane proteins are grown during the 2D crystallization trials of membrane proteins, and helical reconstruction can provide the three-dimensional (3D) structures at atomic resolution in those cases [2]. The resolution of single particle analysis of protein complexes has been improving [3], and an atomic model was recently proposed from a 3D structure determined by this method [4]. While all three of these methods can determine the atomic model from the 3D reconstruction, single particle analysis does not require crystals for the structural determination, and therefore it is considered to be the most general method. In addition, because the particles in different states can be distinguished by image classifications in the single particle method, we can analyze the structures in an equilibrium of different states. Thus, the range of targets for high-resolution structural analysis can be expanded by single particle analysis.

The principle obstacle for high-resolution structural analysis in electron microscopy is irradiation damage of the biological specimen by incident electrons. Cooling the specimen to cryogenic temperatures can reduce the effects of irradiation damage. A comparison of the decay of intensities from tRNA and catalase crystals by electron diffraction revealed that the irradiation damage was reduced to about 1/4 and 1/10 of the value at room temperature,

when the specimens were cooled below 100 K and 20 K, respectively [5]. Therefore, a liquid helium-cooled stage for electron crystallography, where the resolution is mainly determined by electron diffraction patterns, was developed [6], and thus we obtained many atomic models of membrane proteins using the helium stage [7]. Although it is not clear whether the enhanced protection at 20 K is quantitatively the same as in the conditions of electron

microscopy, it may be possible to achieve higher resolution structures by using a liquid helium-cooled stage to minimize the irradiation damage, even in single particle analysis.

To explore this possibility, a new cryo-electron microscope with a liquid helium-cooled stage for single particle analysis was developed and utilized to study the GroEL-GroES-substrate complex. Here we will describe how we optimized the specimen preparation



Fig. 1 The cryo-electron microscope, equipped with a liquid-helium cooled stage, for single particle analysis. The accelerating voltage of the field emission gun is 200 kV, and it is equipped with an 8K × 8K CMOS camera.

2-3-26, Aomi, Koto-ku, Tokyo, 135-0064 Japan

kaorum@ni.aist.go.jp

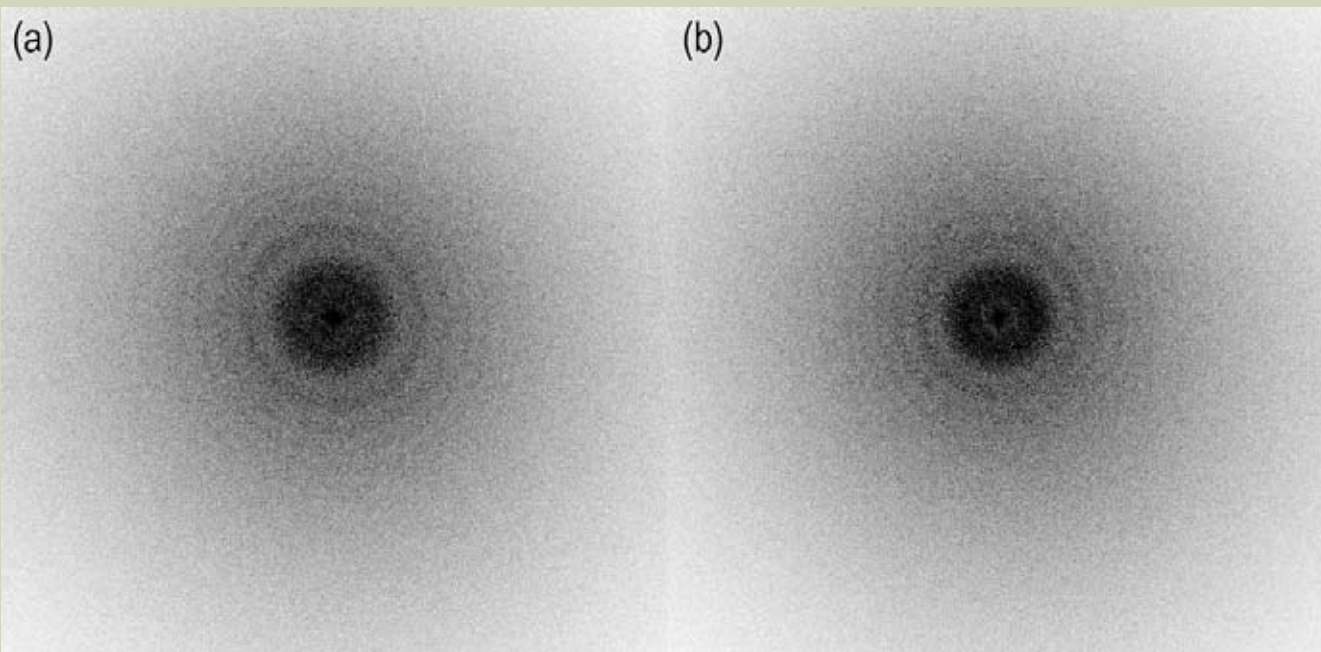


Fig. 2 Typical Fourier transforms from good and poor images. These were calculated from a  $4K \times 4K$  area with a pixel size of about  $1.8 \text{ \AA}$  and a defocus value of about  $2 \mu\text{m}$ . (a) Fourier transforms from a good image. The Thon rings are clear and symmetrical. (b) Fourier transforms from a poor image. The Thon rings do not extend to the higher resolution and are asymmetrical.

for single particle analysis using the liquid-helium cooled stage, and the resulting structure we obtained using the protein complexes from *Thermus thermophilus*. In addition, we recently applied the single particle analysis to the tubular crystals of a membrane protein, and those results will also be discussed.

## Helium-cooled cryo-electron microscope for single particle analysis

While the new JEOL cryo-electron microscope equipped with a liquid-helium cooled stage for single particle analysis has almost the same cryo-stage as those of the cryo-electron microscopes used for electron crystallography [11], the accelerating voltage of the field emission gun is 200 kV, and it is equipped with a CMOS camera with pixel sizes of 8k by 8k (TemCam-F816, TVIPS, Gauting, Germany). The advantage of the 8K camera for single particle analysis is clear. We can collect more particle images from one exposure, and therefore the data collection is more efficient. The choice of the accelerating voltage is also related to the camera. The point-spread function of the camera becomes better at 200kV, as compared with the accelerating voltage of 300 kV, which we usually use for electron crystallography. Therefore, we can use a lower magnification, which also improves the efficiency of the data collection. The new cryo-electron microscope for single particle analysis installed in our institute is shown in **Figure 1**.

In addition, the lower accelerating voltage also enhances the image contrast. At the lower accelerating voltage, more electrons can interact with the materials. The ratio of the intensity formed by zero-loss electrons, which can be used for image formation, to the total intensity of the direct beam can be determined by the

elastic mean free path. The elastic mean free paths in ice for 200 kV electrons and 300 kV electrons are 500 nm and 622 nm, respectively, using equation (1) in Langmore and Smith [12]. Assuming these values and an ice thickness of 100 nm, which is sufficiently large for the size of the GroEL-GroES complex (about 20 nm), the ratios of the electrons used for the imaging are 0.18 and 0.15, respectively.

Since we can irradiate with more electrons when using 300 kV, this comparison is not related to the signal-to-noise ratio. However, this enhancement of the ratio of the image-forming electrons to the total intensity has a clear effect on the image contrast of the GroEL-GroES-substrate complexes. We can calculate the image contrast, using the following equation and the experimental values obtained for the GroEL-GroES complexes,

$$\text{Contrast} = \frac{|Ave_{sg} - Ave_{bg}|}{Std_{bg}}$$

where  $Ave_{sg}$  is the average of the pixel values in the particle images,  $Ave_{bg}$  is the average of the pixel values in the background area, and  $Std_{bg}$  is the standard deviation of the background area. The calculated values are 0.11 and 0.045 for 200 and 300 kV, respectively, and thus the image contrast is much better at 200 kV than at 300 kV. Since the contrast of the cryo-images is very weak, the improvement in the number of electrons for the imaging could clearly enhance the image contrast.

## Sample preparation for helium-cooled cryo-electron microscopy

The preparation of the EM grids to yield good images for image processing, using the liquid helium-cooled stage, is also important. The sig-

nificant difference between the nitrogen and helium temperatures lies in the conductivity of the specimen. Since the resistance of carbon is significantly increased at 4 K, some care must be taken to minimize the beam-induced movement by specimen charging. The procedures described here were developed for the high-resolution image collection from tubular crystals of nicotinic acetylcholine receptor [13], and we used the techniques with only slight modifications. Electron irradiation usually results in charging of biological specimens, which causes beam-induced movement. The inelastic scattering causes the emission of secondary and Auger electrons, which render the specimen positively charged. A clean,  $30 \mu\text{m}$  diameter gold foil objective aperture can be used to emit electrons to neutralize the positive charge.

The preparation of the high conductivity carbon film was also important to minimize the beam-induced movement. When we used Quantifoil R1/4 holey grids (Quantifoil Micro Tolls GmbH, Jena, Germany), we deposited carbon (99.9999% purity) onto the grids, with minimal sparking, in a vacuum of  $<10^{-5}$  mbar during deposition, after washing the Quantifoil grids by immersing them in purified water over several hours. After the deposition, the grids were washed again by immersing them in ethyl acetate for 20 minutes. The carbon-coated grids were then irradiated by 100 kV electrons with a total dose of over  $100 \text{ e}^-/\text{\AA}^2$  for more than 3 hours. This pre-exposure could improve the conductivity of the carbon.

Finally, symmetrical imaging conditions, with the beam entirely covering the hole all the way to the carbon, were used. However, even after these considerations, our ability to obtain good images was still marginal. To evaluate the images, we calculated the Fourier transforms from the center area of the hole. As shown in **Figure 2**, the Fourier transforms calculated from a good image show clear and symmetrical

Thon rings, while the Thon rings from a poor image do not extend to the high-resolution range and are asymmetrical. From this calculation, we can determine the ratio of good images. To achieve a success rate of over 50 % from almost all of the grids after these treatments, we usually use a pre-exposure time of 1.0 second for a 2.0 s exposure. We consider the damage from this irradiation to be acceptable, because of the 2.5-fold reduction in the damage by using liquid helium, as compared to liquid nitrogen.

## Single particle analysis of the GroEL-GroES-substrate complex

We used the microscope and the techniques described above to analyze the structure of the GroEL-GroES-substrate complex [14]. GroEL is a molecular chaperone, which helps other proteins to fold properly, and is called a chaperonin. It works as an essential mediator for folding in eubacteria, mitochondria, and chloroplasts. The co-chaperonins GroES and ATP are required for GroEL to exert its full activity, and they form a large complex [15]. The complex consists of two heptameric rings of GroEL stacked back-to-back and seven subunits of GroES, which form a dome-shaped structure on top of the GroEL rings. The formation of this complex creates a large hydrophilic cavity, and the folding polypeptide is considered to be encapsulated in the cavity so that it can be correctly folded into the native conformation without the risk of aggregation. However, the folding substrate inside the cavity has never been visualized. Therefore, we used the native chaperonin complex from *Thermus thermophilus*, a thermophile, to visualize the substrate inside the cavity, because the complex from the thermophile is quite stable, and at least 24 different substrate proteins were identified from the purified complexes.

The structures of GroEL and its complexes have been studied extensively by single particle analysis [16]. Single particle analysis by cryo-electron microscopy has the advantage that it can solve the structure under any solution conditions. In addition, heterogeneous samples can be analyzed by this method, because the averaged structure of the similar but heterogeneous specimens can be calculated, and the images can be classified into several different structures. Thus, it could be much easier to calculate the intermediate structures by single particle analysis, rather than crystallographic methods. Here we averaged the complex with different folding substrates, because many different folding substrates are folded by GroEL. However, the classification of several different structures and the calculation of those structures are also possible using GroEL, and those results were published at almost the same time as our result [17].

We accumulated 28,188 particle images, which were selected as GroEL-GroES complexes as judged from their shape, using 336 pictures, and performed the single particle analysis. The 2D alignment and classification processes were performed by the MRA and MSA techniques, using the IMAGIC program packages. The parameters for CTF correction were determined by *ctfit* in the EMAN package. The 3D structure of the complex, which was calculated by the 3D filtered back projection, is

shown in **Figure 3**. The reconstructed 3D map clearly showed a density corresponding to the substrate proteins at almost the center of the cavity. A comparison of the GroEL-GroES complex with that from *E. coli*, which was reconstructed without the folding substrates, confirmed that the density in the cavity was not observed for *E. coli* complex, and therefore it is not an artifact from image processing.

This density is located in the center of the cavity and is surrounded by acidic residues. Since this density is the average of many substrates, the fine details about their interactions with the chaperonin are unknown. However, considering the result that the density is not scattered throughout the cage, but is concentrated in the center of the cavity, the majority of the substrate proteins are restricted in a limited space. Thus, the observed position of the substrates indicates the electrostatic repulsion effects for most of the GroEL substrates. In fact, most GroEL substrates have a negative net charge. The protein folding might be assisted by this interaction between the interior walls of the cavity and the substrate proteins.

## Application of single particle analysis to the tubular crystal of a membrane protein

The single particle method can be applied not only to protein complexes but also to various samples. For example, the 3D structures of the tubular crystals of membrane proteins can be analyzed by modifying this method. Iterative helical real-space reconstruction (IHRSR) uses single-particle image analysis, in combination with imposed real-space helical symmetry, to allow the effective analysis of tubular crystals with such properties as poorly ordered helical symmetry, bent tubes, or low signal-to-noise ratios on electron microscopy images [18]. Here, we show the 3D structure of the membrane domain of erythrocyte band 3 in an inhibitor-stabilized, outward-open conformation at 18 Å resolution, which was determined by this method [19].

Erythrocyte band 3 (anion exchanger 1, or AE1) mediates the electroneutral exchange of ions such as chloride and bicarbonate across the erythrocyte plasma membrane. Band 3 contains functionally independent cytoplasmic and membrane domains. The cytoplasmic domain functions to anchor the cytoskeleton to the plasma membrane, while the membrane domain allows anion exchange. We purified the band 3 protein with the anion transport inhibitor 4,40-diisothiocyanatodihydrostilbene-2,20-disulfonic acid (H<sub>2</sub>DIDS). Stilbene compounds, such as H<sub>2</sub>DIDS, reportedly stabilize band 3 in the outward-open form. Using the purified H<sub>2</sub>DIDS-bound, outward-open membrane domain of band 3 (hB3MD) and a dialysis procedure, we obtained tubular crystals with a diameter of 37 nm, and applied IHRSR to the crystals.

**Figure 4** shows the overall 3D map of the band 3 tubular crystal. Two hB3MD molecules, which form a dimer, are enclosed within blue and green boxes. All of the hB3MD dimers in the tubular crystals are oriented in the same direction relative to the tube axis and appear to be in close contact with each other. An immunoelectron microscopy analysis using 2A8 IgG antibodies revealed that the outer and inner surfaces of the tubular crystal corresponded to the

intracellular and extracellular portions of hB3MD, respectively. The membrane domain of band 3 is thought to consist of several subdomains, because a projection image of the 3D map of the hB3MD dimer perpendicular to the membrane plane showed two high-density regions, suggesting that the domain is composed of at least two subdomains. However, it is currently not possible to determine which segment of the molecule belongs to each subdomain. The anion transport mechanism of band 3 has been explained by a "ping-pong" model, which postulates that there is only one transport site, which faces either intracellularly (inward-open form) or extracellularly (outward-open form). Conformational changes between these forms only occur if a substrate is bound to the transport site. The 3D structure of the outward-open form, which consists of at least two domains, is consistent with this model, but a higher resolution structure is required to determine the relationship between the structural features revealed here and the function of band 3.

## Conclusion

A new JEOL cryo-electron microscope, equipped with a liquid-helium cooled stage, was developed and used for the structural analysis of the GroEL-GroES-substrate complex and the 3D reconstruction from tubular crystals of human erythrocyte band 3 membrane protein. These results clearly showed the benefits of applying single particle analysis to various heterogeneous samples. The advantages of the liquid-helium cooled stage for single particle analysis should be explored in future experiments. Further improvements in sample preparation and image collection at the liquid helium temperature will enable higher resolution structural analyses by the single particle method.

## Acknowledgments

The author would like to thank all of the collaborators who performed the studies described here, who are authors in the referenced papers. The development of the microscope and these studies were supported by NEDO grants.

## References

- [1] T. Gonen, Y. Cheng, P. Sliz, Y. Hiroaki, Y. Fujiyoshi, S. C. Harrison, T. Walz, *Nature*, **438**, 633, (2005)
- [2] A. Miyazawa, Y. Fujiyoshi, N. Unwin, *Nature*, **423**, 949, (2003)
- [3] X. Yu, L. Jin, Z. H. Zhou, *Nature*, **453**, 415 (2008)
- [4] J. Zhang, M. L. Baker, G. F. Schröer, N. R. Douglas, S. Reissmann, J. Jakana, M. Dougherty, C. J. Fu, M. Levitt, S. J. Ludtke, J. Frydman, W. Chiu, *Nature*, **463**, 379, (2010)
- [5] Y. Fujiyoshi, *Adv. Biophys.*, **35**, 25, (1998)
- [6] Y. Fujiyoshi, T. Mizusaki, K. Morikawa, H. Yamagishi, Y. Aoki, H. Kihara, Y. Harada, *Ultramicroscopy*, **38**, 241, (1991)
- [7] Y. Kimura, D. G. Vassilyev, A. Miyazawa, A. Kidera, M. Matsushima, K. Mitsuoka, K. Murata, T. Hirai, Y. Fujiyoshi, *Nature*, **389**, 206, (1997)
- [8] K. Murata, K. Mitsuoka, T. Hirai, T. Walz, P. Agre, J. B. Heymann, A. Engel, Y. Fujiyoshi, *Nature*, **407**, 599, (2000)

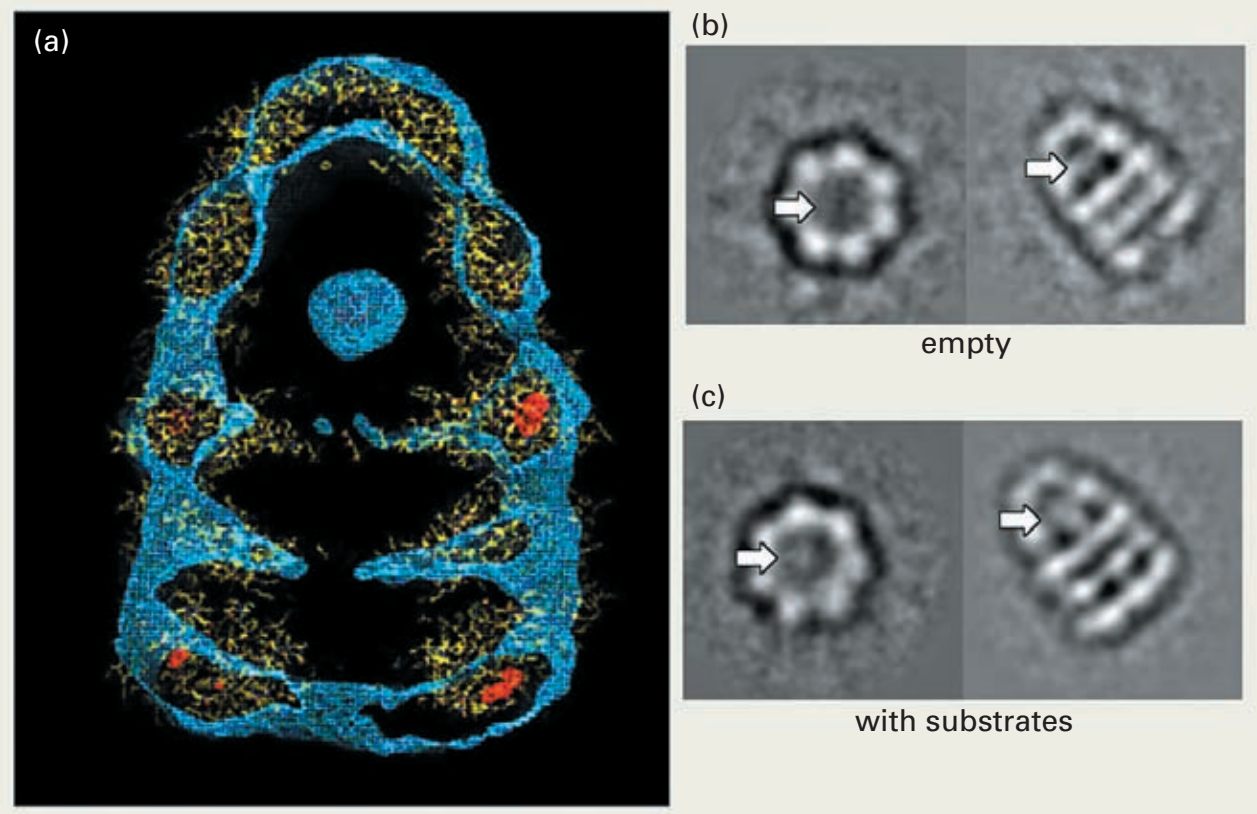


Fig. 3 The overall structure of the GroEL-GroES-substrate complex. (a) Side view of the 3D map, and the fitted atomic model. (b) Comparison of the empty chaperonin complex from *E. coli* with the native complex from *Thermus thermophilus*.

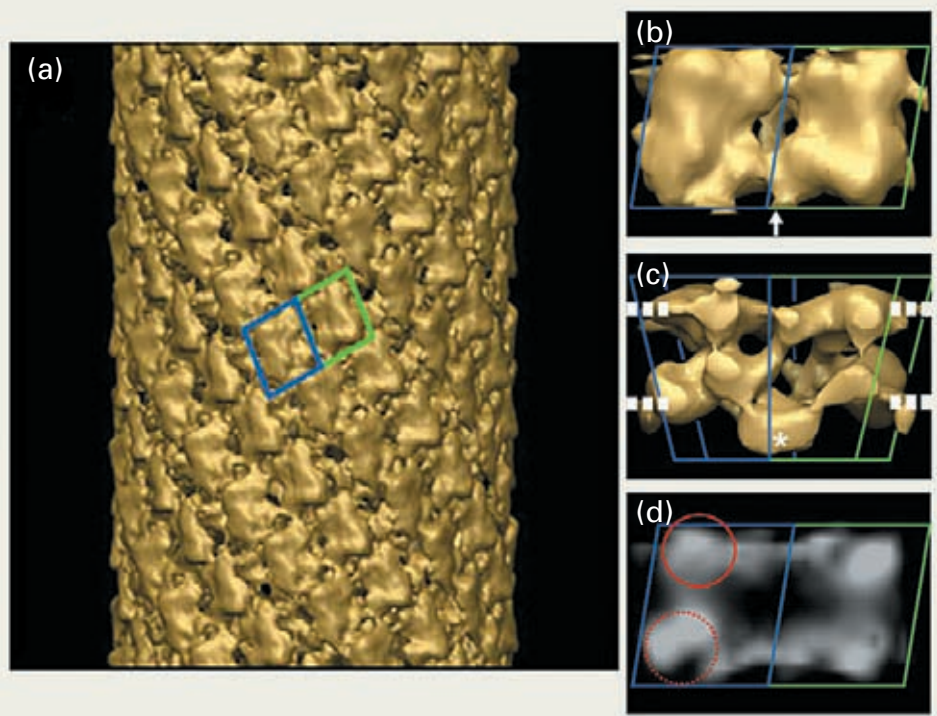


Fig. 4 The 3D image reconstruction of the hB3MD tubular crystal. (a) Side view of the tubular crystal. Two molecules in a possible dimer are enclosed in blue and green boxes. (b) The intracellular surface of a unit cell containing an hB3MD dimer. (c) The 3D map of an hB3MD dimer, viewed in the direction parallel to the tube axis. (d) Projection image of the 3D map from the intracellular side. The two high-density regions are indicated by solid and dashed red circles, to suggest the presence of two subdomains.

- [9] Y. Hiroaki, K. Tani, A. Kamegawa, N. Gyobu, K. Nishikawa, H. Suzuki, T. Walz, S. Sasaki, K. Mitsuoka, K. Kimura, A. Mizoguchi, Y. Fujiyoshi, *J. Mol. Biol.* **355**, 628, (2006)
- [10] P. J. Holm, P. Bhakat, C. Jegerschöld, N. Gyobu, K. Mitsuoka, Y. Fujiyoshi, R. Morgenstern, H. Hebert, *J. Mol. Biol.* **360**, 934, (2006)
- [11] C. Jegerschöld, S. C. Pawelzik, P. Purhonen, P. Bhakat, K. R. Gheorghe, N. Gyobu, K. Mitsuoka, R. Morgenstern, P. J. Jakobsson, H. Hebert, *Proc. Natl. Acad. Sci. USA.* **105**, 11110, (2008)
- [12] J. P. Langmore, M. F. Smith, *Ultramicroscopy*, **46**, 349, (1992)
- [13] A. Miyazawa, Y. Fujiyoshi, M. Stowell, N. Unwin, *J. Mol. Biol.*, **288**, 765, (1999)
- [14] R. Kanno, A. Koike-Takeshita, K. Yokoyama, H. Taguchi, K. Mitsuoka, *Structure*, **17**, 287, (2009)
- [15] Z. Xu, A. L. Horwich, P. B. Sigler, *Nature*, **388**, 741, (1997)
- [16] S. J. Ludtke, D. L. Chen, J. L. Song, D. T. Chuang, W. Chiu, *Structure*, **12**, 1129, (2004)
- [17] D. K. Clare, P. J. Bakkes, H. van Heerikhuizen, S. M. van der Vies, H. R. Saibil, *Nature*, **457**, 107, (2009)
- [18] E. H. Egelman, *J. Struct. Biol.* **157**, 83, (2007)
- [19] T. Yamaguchi, T. Fujii, Y. Abe, T. Hirai, D. Kang, K. Namba, N. Hamasaki, K. Mitsuoka, *J. Struct. Biol.*, **169**, 406, (2010)